Mechanisms for the behavior of carbon films during annealing

D. G. McCulloch and J. L. Peng
Department of Applied Physics, RMIT University, GPO Box 2476V, Melbourne 3001, Australia

D. R. McKenzie
School of Physics (A28), University of Sydney, NSW 2006, Australia

S. P. Lau, D. Sheeja, and B. K. Tay
School of Electrical and Electronic Engineering, Nanyang Technological University, Singapore 639798
(Received 2 December 2003; revised manuscript received 10 March 2004; published 11 August 2004)

The effect of annealing on 1 μm thick single and multilayer amorphous carbon (*a*-C) films prepared by filtered cathodic arc is investigated. Single layer films, with a sp^2 to sp^3 bonding fraction of approximately 50% increase their level of compressive stress following annealing. Multilayer films—consisting of alternating layers of high sp^3 fraction (tetrahedral amorphous carbon, ta-C) and intermediate sp^3 fraction show a decrease in compressive stress following annealing. Using cross-sectional transmission electron microscopy, we show that the single layer films and the intermediate sp^3 layers in the multilayer films develop a strong preferred orientation with graphite-like layers aligned perpendicular to the film surface. The ta-C layers in the multilayer films develop the opposite preferred orientation near their top interfaces. We conclude that these preferred orientation effects are linked to the stress profile of the structures. We propose an underlying mechanism for the annealing effects of *a*-C films based on *ab initio* calculations. In order to minimize total energy, intermediate sp^3 films will either decrease their sp^3 fraction and generate stress or increase their sp^3 fraction and relieve stress. On the other hand, high sp^3 films retain their high sp^3 fraction following annealing.

DOI: 10.1103/PhysRevB.70.085406 PACS number(s): 61.43.−j, 81.05.Uw, 81.15.Aa

I. INTRODUCTION

The reduction of stress in amorphous carbon (*a*-C) films is important for practical applications. Tetrahedrally bonded amorphous carbon (ta-C)[1] has applications as a hard, wear resistant coating, and potentially as an electronic material. The high level of intrinsic compressive stress limits the thickness of ta-C films to approximately 100 nm. Recent work has shown that the use of pulsed biasing during deposition can be used to control stress[2–4] although this is accompanied by a reduction in the sp^3 fraction. Another method of reducing the stress which can be used after deposition is annealing at temperatures between 200 and 700 °C.[3,5–8] Under some conditions, the sp^3 bonding fraction of ta-C can be retained during this annealing step.[5–8] Films with intermediate sp^3 content, in the region of 50%, show a very different behavior in which there is strong stress generation rather than stress relief.[3,7] There is no widely accepted mechanism to describe this variation in stress for different types of *a*-C following annealing.

In previous work on *a*-C of low to intermediate sp^3 fraction prepared under ion bombardment, a preferred orientation in graphite-like layers has been observed.[9] This preferred orientation results in the layers aligning themselves in the direction parallel to the direction of the incident ions (normally normal to the surface). There is debate as to the driving force behind this phenomenon in carbon and related materials.[10] One view is that it is essentially a response to an anisotropic stress field to minimize elastic strain energy[9,11] and another view is that it arises principally from dynamic processes such as selective sputtering or ion channeling.[12]

In this work we examine the effects of annealing on preferred orientation in *a*-C films by carrying out detailed microstructural studies using transmission electron microscopy (TEM) and electron energy loss spectroscopy (EELS). We first study the effects of annealing on relatively thick single layer films of intermediate sp^3 fraction prepared using ion bombardment during film growth. In addition, we study the annealing behavior of multilayer carbon film consisting of intermediate sp^3 fraction alternating with layers of high sp^3 fraction (ta-C). These multilayer structures provide an opportunity to investigate the behavior of *a*-C of different sp^3 fraction subjected to precisely the same annealing treatment. In particular, we can study the development of preferred orientation in the absence of ion bombardment. As a means of investigating the energetics of the annealing process, we apply additional results from previously published *ab initio* molecular dynamics calculations[13] to low, intermediate, and high sp^3 fraction *a*-C.

II. EXPERIMENTAL AND THEORETICAL METHODS

Films were deposited on silicon substrates using a filtered cathodic vacuum arc system which is described in detail elsewhere.[14] A 99.999% pure graphite target was employed with an arc current of 70−80 A. The silicon substrates were placed in the deposition chamber and pumped down to a base pressure of better than 3×10^{-5} Pa. The deposition system was also equipped with a plasma immersion ion implantation system (PIII),[15] which allows pulsed high voltage to be supplied to the substrate. Prior to film growth, the silicon substrates were cleaned using an Ar plasma. Two types of thick amorphous carbon samples were prepared. First, an approximately 1 μm thick amorphous carbon sample was prepared by applying a 3 kV, 25 μs pulse at a frequency of

600 Hz to the substrate. A second film of similar thickness was also prepared in the form of a multilayer with 20 alternating low and high density layers. The low density (intermediate sp^3 fraction) layers nominally 38 nm thick were prepared with pulse parameters of 3 kV, 600 Hz, and 25 μs. The high density (ta-C) layers nominally 76 nm thick were prepared without PIII under floating bias conditions.

The intrinsic stress in the deposited films was determined from the curvature of the substrate and applying Stoney's equation.[16] The annealing was performed using a rapid thermal annealing system with a base pressure of 10^{-4} Pa. Samples were annealed at 200 and 600 °C for up to 7 min.

Samples were prepared for cross-sectional TEM by initial mechanical polishing using a tripod polisher, and finally thinning to electron transparency using a GATAN dual ion mill model 600 ion beam thinner as well as a GATAN precision ion polishing system model 691. The samples were then analyzed using a JEOL 2010 TEM operating at 200 kV. EELS was performed using a GATAN imaging filter. The fraction of sp^2 bonded carbon atoms was calculated from the carbon *K* edge as described elsewhere.[17]

In this paper, we apply results from previous *ab initio* Car-Parrinello molecular dynamics liquid quench simulations of *a*-C.[13] In particular, we calculate the energy/atom at the various densities simulated after correcting to account for finite basis set effects. The zero of energy was taken to be the energy per atom of a crystalline diamond calculation performed under the same simulation conditions.

III. RESULTS AND DISCUSSION

A. Single layer samples

Figure 1(a) shows the compressive stress for the as-deposited single layer *a*-C film, and the stress following annealing at temperatures of 200 and 600 °C as a function of annealing time. The stress was observed to increase significantly at both temperatures, even for annealing times of only 2 min, and then the stress asymptotes to approximately 2.4 GPa at both annealing temperatures. Therefore, during annealing, the stress level has increased by approximately 2 GPa. This effect has been observed previously for films of intermediate sp^3 fraction[7] and is at first sight a surprising result since the spontaneous appearance of elastic strain energy appears to violate the principle that free energy should be minimized.

Figure 2 shows cross-sectional TEM (XTEM) images of the single layer (intermediate sp^3) *a*-C films both before and after annealing to temperatures of 200 and 600 °C. The films were found to be largely uniform in thickness and Table I shows the average change in film thickness following annealing. It was found that for the single layer film, there was an increase in film thickness of $6 \pm 2.5\%$ following annealing. Also shown in Fig. 2 are selected area diffraction patterns taken from each film. The diffraction pattern from the as-deposited sample shows the typical diffuse ring pattern expected from an amorphous sample. After the 600 °C anneal the diffraction pattern exhibits strong arcs on the rings in the vicinity of the graphite-like {002} reflections. The diffraction patterns are correctly aligned with respect to the image in each case so that the arcs reveal the presence of a strong preferred orientation of graphite-like layered structures with their planes perpendicular to the film surface. This result is significant to the debate on the origin of similar preferred orientation in *a*-C and boron nitride developed under ion beam bombardment.[18] Such an orientation occurs, for example, when glassy carbon is ion implanted[9] and has been observed in boron nitride films[19,20] grown under ion impact. The debate is centered on whether the preferred orientation arises as a response to the biaxial compressive stress field generated by the ion impacts or from dynamical effects associated with the bombardment itself. The result presented here clearly rules out the latter. The preferred orientation develops in the absence of any ion bombardment, consistent with it being a response to the spontaneously appearing compressive stress.

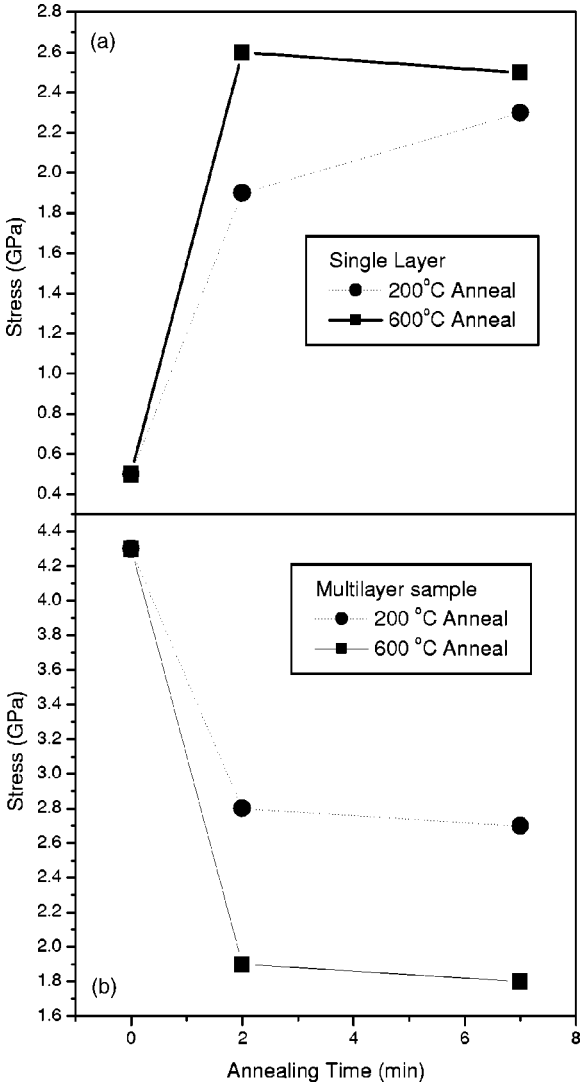

FIG. 1. The intrinsic stress of the: (a) as-deposited single layer and (b) multilayer films as a function of annealing time and temperature.

Figures 3(a) and 4(a) compare the low loss and C *k*-edge EELS spectra for the as deposited and 600 °C annealed samples. The presence of a $\pi - \pi^*$ feature at about 5 eV and a sharp 1 $s - \pi^*$ peak at 285 eV following annealing reflect

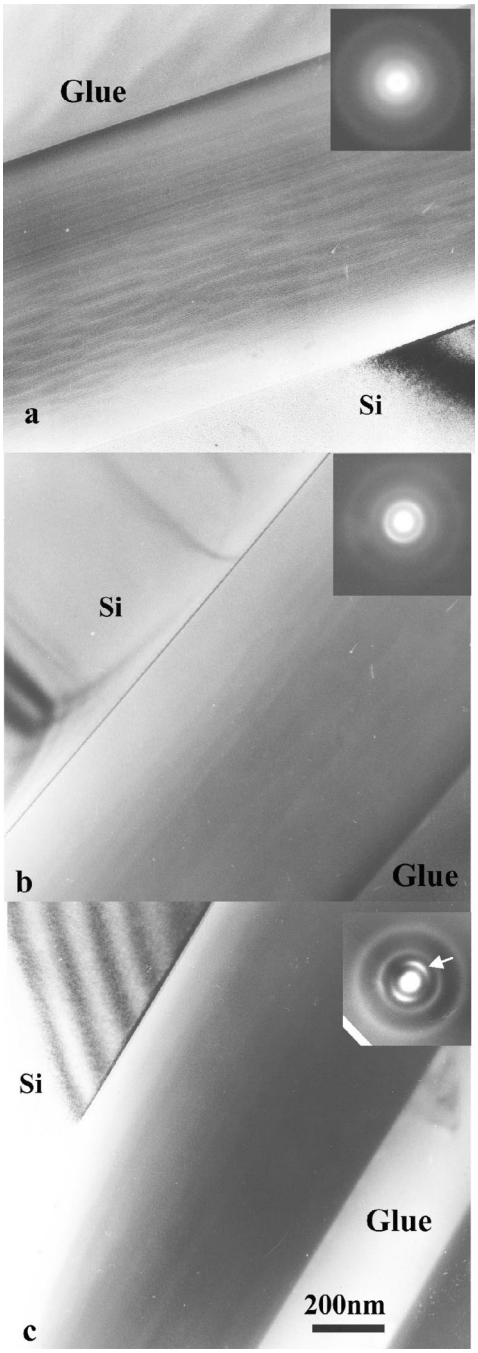

FIG. 2. Cross-section TEM images and selected area diffraction patterns from (a) the as-deposited single layer film and the single layer film following annealing at (b) 200°C and (c) 600°C for 7 min. The arrow in (c) indicates the preferred orientation arc at the location of the graphite-like {002} reflection.

the growth of graphite-like layers. Table I summarizes the results of the EELS analysis on each of the carbon films. The plasmon energy may be used to approximate the volume density.[21] Table I lists the volume densities calculated from the plasmon peak positions assuming four valence electrons per atom and using a calibration factor which has been found to work well for graphite and diamond.[22] The as deposited film was found to have a plasmon energy of 26.9 eV and a $sp+sp^2$ bonding fraction of 50%. Following annealing at 200°C, the plasmon energy decreases to 25.7 eV and the $sp+sp^2$ bonding fraction increases to 60%. After annealing at 600°C, the plasmon energy is found to be similar at 25.8 eV while the $sp+sp^2$ bonding fraction is increased further to 80%. The EELS results are consistent with an increase in sp^2 bonding within the layer as the annealing temperature is increased. An increase in sp^2 bonding should result in a decrease in film density, which is reflected in the decrease in plasmon energy from the initial value. We propose that the increase in stress is a direct result of this decrease in density, which leads to an increase in the volume of the film. The film is attached to the substrate but can flow upwards as it has a free surface. After the expansion a biaxial compressive stress will appear in the plane of the film corresponding to the yield stress required to induce the upward flow. Dark field images taken with an objective aperture positioned over one of the preferred orientation arcs shown in the diffraction pattern for the 600°C annealed sample [Fig. 2(c)] showed oriented graphite-like regions are scattered through the entire film thickness. These oriented graphite-like regions develop as a response that helps to reduce the buildup of strain energy in the biaxial stress field.[11]

B. Multilayer samples

Figure 1(b) shows the compressive stress for the as-deposited multilayer film, and the stress following annealing at temperatures of 200 and 600°C as a function of annealing time. In contrast to the single layer case, the stress decreases significantly from 4.3 to approximately 2.8 GPa following annealing at 200°C and approximately 1.8 GPa following annealing at 600°C. The stress level of the as deposited film is an average of the intrinsic stress present in the ta-C layers, approximately 9 GPa,[3] and the *a*-C layers of 0.5 GPa as reported in Sec. III A. This gives a value of 4.25 GPa, close to the measured values of 4.3 GPa for the multilayer film. According to reports in the literature,[8] the stress level in the ta-C should decrease to 0.1 of its initial value after the 600°C anneal. The *a*-C layer will increase its stress to 2.4 GPa (according to Sec. III A) giving an overall value of 1.65 GPa. This is in good agreement with the measured stress level of the multilayer film.

Figure 5 shows XTEM images and diffraction patterns from the multilayer films both before and after annealing. A series of alternating dark and bright bands are clearly visible within the film corresponding to layers produced with and without PIII. Diffraction patterns from each film are also shown and demonstrate the development of preferred orientation, similar in nature to that observed in the case of single layer films.

EELS analysis was performed on the multilayer samples and the results for the as deposited and 600°C samples are shown in Figs. 3 and 4. In addition, some of the key properties are summarized in Table I. In the as-deposited sample, the dark bands associated with layers produced without PIII were found to have a plasmon energy of 29.5 eV and an $sp+sp^2$ fraction of 35%, indicating that the dark layers have a high density and a high proportion of diamond-like bonding. The bright layers were found to have a plasmon energy

TABLE I. Summary of the samples examined and some important experimentally determined parameters. The change in layer thicknesses following annealing was calculated by averaging measurements from several locations on each sample. The density was estimated from the plasmon peak position and the sp^2 bonding fraction measured from the carbon *K* edge using EELS.

Sample type	Annealing temp (°C)	Stress (GPa)	Layer type	Change in layer thickness (±2.5%)	Plasmon peak position (eV) (±0.2)	Density (g/cm^3)	Fraction of sp^2 bonding (±0.05)
Single layers	—	0.6	—	—	26.9	2.3	0.50
	200	2.2	—	+4%	25.7	2.0	0.60
	600	2.5	—	+6%	25.8	2.1	0.80
Multilayers	—	4.3	High density	—	29.5	2.7	0.35
			Low density	—	27.0	2.3	0.50
	200	2.7	High density	−4%	29.7	2.7	0.30
			Low density	+10%	25.9	2.1	0.60
	600	1.8	High density	0%	30.0	2.8	0.25
			Low density	+20%	25.8	2.0	0.75

of 27.0 eV and a $sp+sp^2$ bonding fraction of 50%, consistent with the as-deposited single layer film which was prepared under identical conditions. Following annealing, the low density layers develop a $\pi-\pi^*$ peak and sharp $1s-\pi^*$ peak that was observed in the single layer films. The plasmon energy of the low density layers decreases to 25.8 eV and the $sp+sp^2$ bonding fraction increased to approximately 75%, again following the trend found in the case of the single layer film prepared under similar conditions.

In the case of the high density layers, the $sp+sp^2$ bonding fraction reduces and the plasmon peak energy increases slightly following annealing. This result is consistent with previous work which showed that ta-C is resistant to major structural change for annealing up to 600°C.[7,8] The increase in plasmon peak position following annealing indicates that some structural rearrangement has occurred which results in an increase in the density and diamond-like bonding.

Table I provides information on the average changes in low and high density layer thicknesses in the multilayer film following annealing. The thickness of the high density layers remains relatively constant while the low density layers become thicker. After annealing at 600°C, the low density layers swell by about 20%. This result is consistent with the decrease in the density of these layers indicated by the reduction in their plasmon energy.

Figure 6(a) shows a dark field image of several layers from the 600°C annealed sample taken with an objective aperture positioned over one of the preferred orientation arcs shown in the diffraction pattern for Fig. 5(c). This figure shows that as for the single layer case, graphite-like structures oriented with planes perpendicular to the film surface are scattered throughout the interior of the low density layers. Figure 6(b) shows a dark field image with the aperture positioned on the {002} ring at a position 90° to the arc. The thin bright lines shown in Fig. 6(b) correspond to the case in which graphite-like layers are aligned with their basal planes parallel to the surface of the sample. This corresponds to the lowest energy surface in graphite and is expected to occur at an interface or surface where there is a little strain energy present. Figure 6(b) also shows dark lines inside the low density layers immediately next to the interface with high density layers. These correspond to an especially strong orientation of graphite-like layers perpendicular to the film surface. A high resolution image taken near the interface between bright and dark layers is shown in Fig. 7. Near this interface, a line of {002} graphite-like fringes can clearly be observed.

A schematic of the observed preferred orientations is shown in Fig. 6(c). These observations are a consequence of the stress-distance relation in Fig. 6(d) developed from the knowledge of the annealing behavior of single layers of each material. The low density layers after annealing have developed a high level of compressive stress while the sp^2 fraction has increased. In order to accommodate this increase in stress the orientation of the graphite-like crystallites will be such as to minimize their strain energy as in the single layer case. This energy minimization is particularly strong near the interfaces and allows a rapid reduction in stress at the interface. Note that the surface of a single layer has a different boundary condition than the interfaces in a multilayer structure. While vertical movement is allowed in both cases, buried interfaces are constrained laterally. This is only important when comparing the very surface of a film with an interface.

Just inside the high density layers, the stress falls to very low levels, allowing the opposite orientation of graphite-like layers to occur. Equivalent dark field images taken from the same positions on the {002} ring of the as deposited sample revealed no evidence of preferred orientation. However, it is likely that graphite-like layers oriented parallel to the surface exist on the top surface of ta-C layers immediately after growth since this orientation is expected to have the lowest surface energy.

C. A mechanism for changes in stress and preferred orientation in carbon films

The total internal energy of a film can be written as a sum of contributions from the bonding energy between atoms in an unstressed state and the elastic strain energy. The strain energy can be related to the volume (V), pressure (P), and

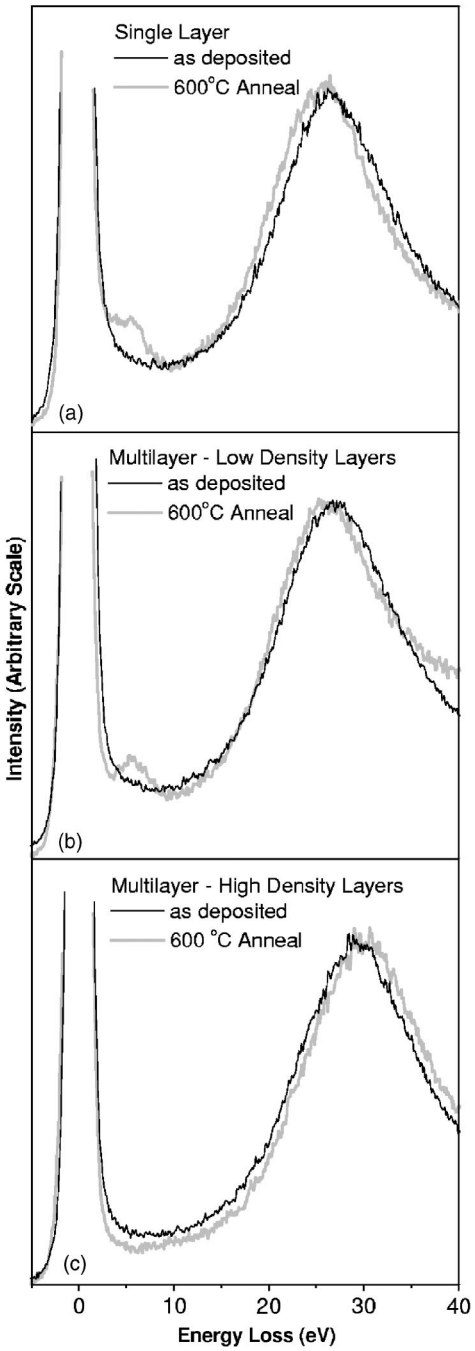

FIG. 3. A comparison of the low loss EELS spectra for the: (a) single layer and (b) and (c) multilayer films before and after annealing at 600°C for 7 min.

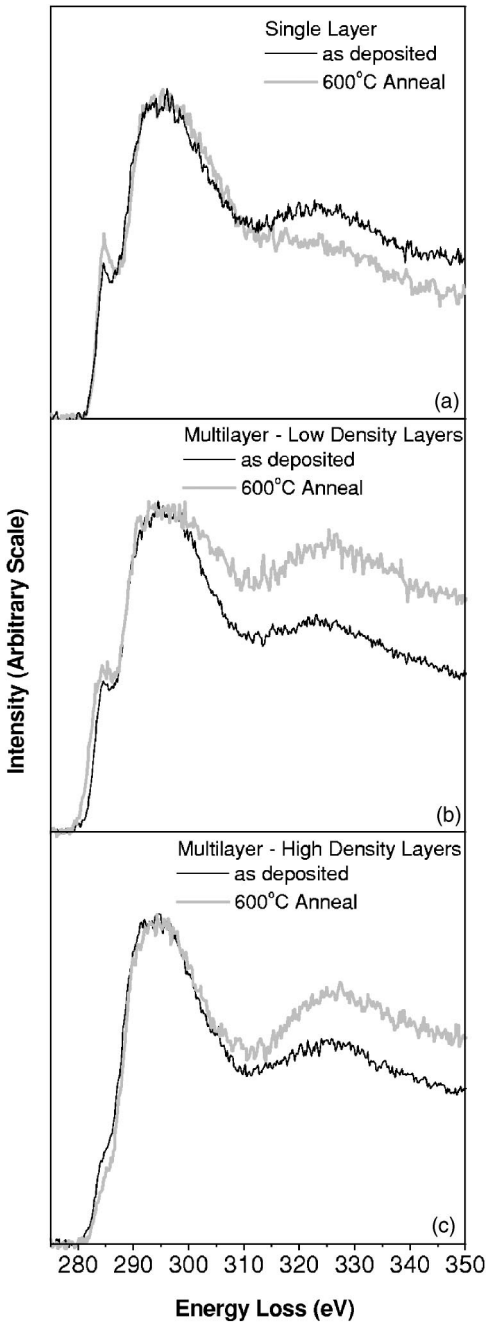

FIG. 4. A comparison of the EELS spectra in the vicinity of the C *k* edge for the: (a) single layer and (b) and (c) multilayer films before and after annealing at 600°C for 7 min.

bulk modulus (B), giving the following expression for the total internal energy from thermodynamics:

$$E_{\text{internal}} = E_{\text{bonding}} + \frac{VP^2}{2B}. \tag{1}$$

Annealing at high temperature gives mobility to the atoms and allows the system to reduce its total internal energy.

We first consider the case of a film being annealed in a detached condition from the substrate. The only energy contribution is then from the bonding energy of the unstressed state of the interior. This will depend on the detailed microstructure and we expect the system to reconfigure after annealing in such a way that its total energy is reduced. When the film is annealed while still attached to the substrate, the constraint on the film area also leads to the minimization of the internal energy, but less work is done by the film in expanding or contracting. The constraint may mean that the internal energy contains some elastic strain energy contribution, both before and after annealing.

Figure 8 shows the energy per atom relative to diamond for a range of amorphous carbon networks produced using *ab initio* Car-Parrinello molecular dynamics liquid quench

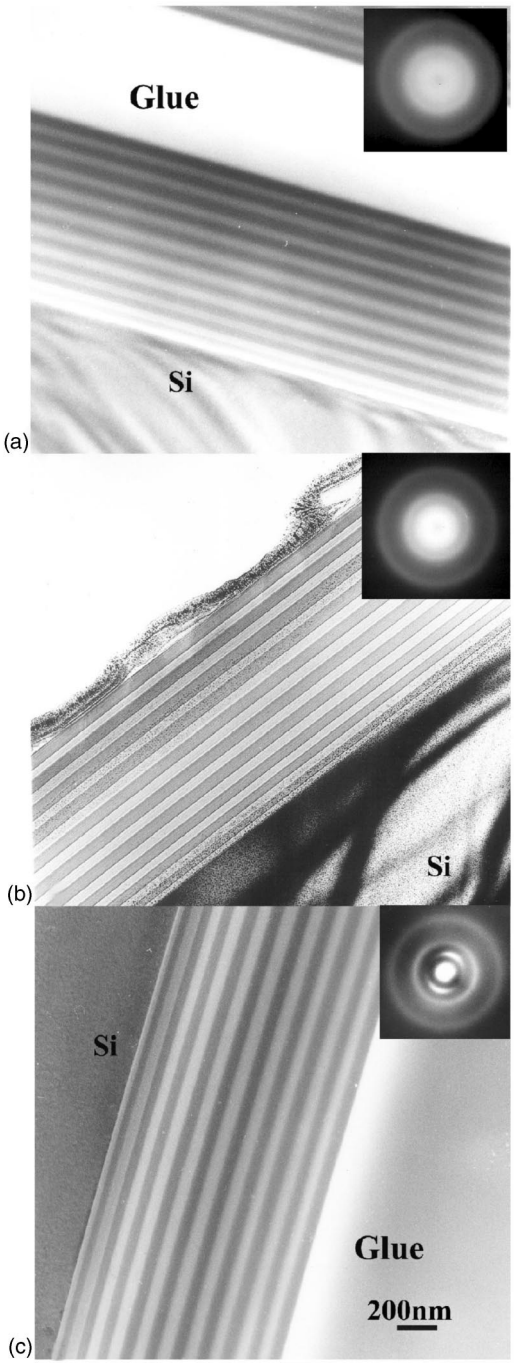

FIG. 5. Cross-section TEM image and selected area diffraction patterns from (a) the as-deposited multilayer film and the multilayer film following annealing at: (b) 200 °C and (c) 600 °C for 7 min.

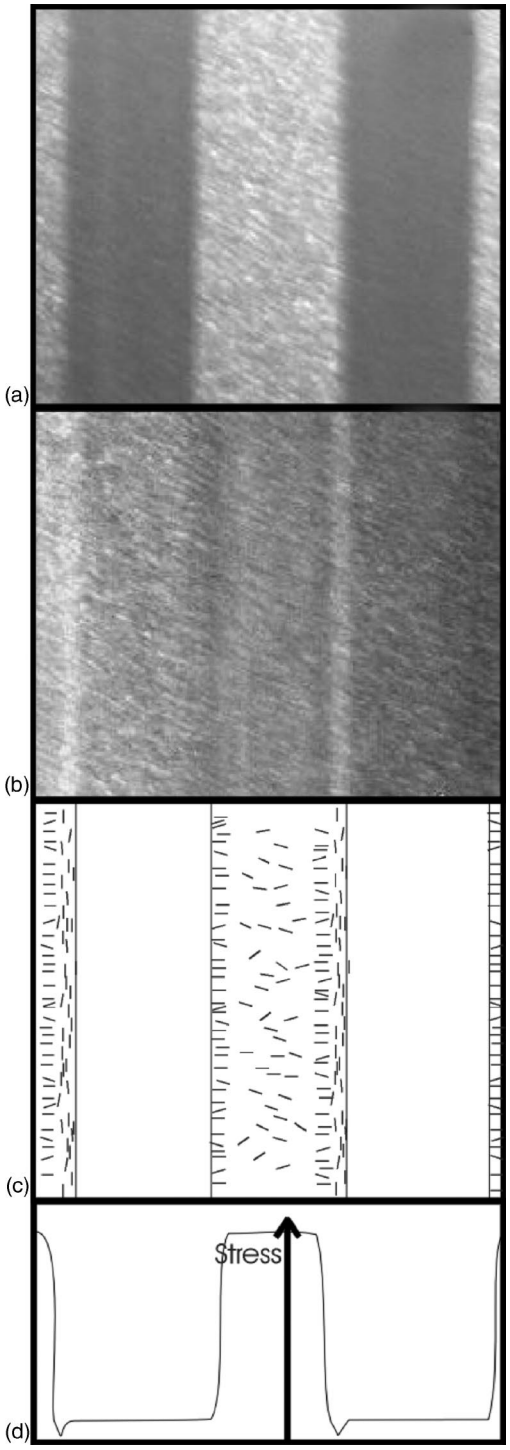

FIG. 6. (a) Dark field image of the multilayer film annealed at 600 °C taken using the preferred orientation {002} arc shown in Fig. 5(c). (b) The corresponding dark field image taken from the {002} graphitic ring at a position 90° from the arc. (c) Schematic representation of the orientation of {002} graphitic planes for the layers shown in (a) and (b). A sketch of the stress distance relation through the layers is shown in (d).

calculations.[13] These simulations were done under constant volume conditions and a hydrostatic pressure P is present after the quenching process. It is convenient to reduce all simulations to a common stress state for comparison purposes. This can be done by subtracting the strain energy term of Eq. (1) using an estimate of the bulk modulus, calculated to be 310 GPa for a 2.9 g/cm^3 simulation.[23] The resulting internal energy without a strain energy contribution is also shown in Fig. 8.

The plot in Fig. 8 can now be used to predict how amorphous carbon films of various sp^3 fractions will behave after annealing. A film corresponding to point A in Fig. 8 of low sp^3 fraction will, after annealing, move to an even lower sp^3

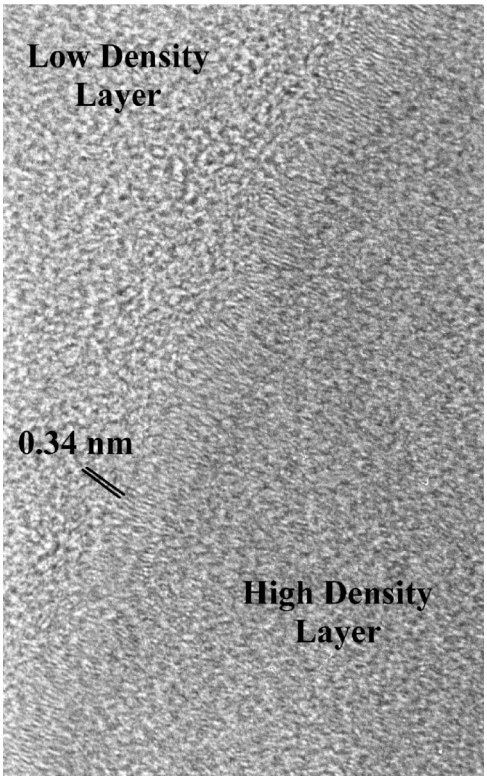

FIG. 7. High-resolution image in the vicinity of a low density/high density interface in the multilayer film annealed at 600°C. Graphite-like {002} fringes with a spacing of approximately 0.34 nm aligned perpendicular to the film surface can be seen running down this interface.

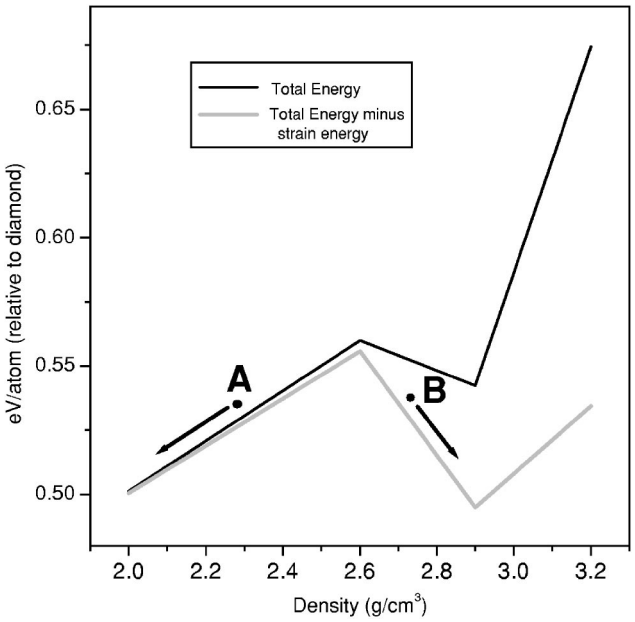

FIG. 8. The energy per atom for a range of 125 atom amorphous carbon networks produced using *ab initio* Car-Parrinello molecular dynamics liquid quench calculations (Ref. 13). The zero of energy is chosen to be the energy per atom of crystalline diamond calculated under the same simulation conditions. Also shown is the resulting energy after subtracting the strain energy given by Eq. (1). The movement direction for two films with densities at points A and B are shown following annealing.

fraction, expanding and generating stress in the process. This situation is illustrated in the case of the single layer *a*-C film in this work, which has a density of approximately 2.3 g/cm^3 (see Table I). After annealing, this film will reduce its energy per atom and according to Fig. 8, this will result in a decrease in density and an increase in sp^2 bonding. There will be a corresponding increase in elastic strain energy which can be calculated using Eq. (1). The increase in stress of 2 GPa observed in this case following annealing would result in an increase in the overall energy of only 6×10^{-4} eV/atom. Therefore, the energy penalty for generating stress as the structure rearranges into the lowest energy configuration is smaller than the energy release resulting from the microstructural rearrangements.

The level of stress generated in this way is ultimately limited by the amount needed to compress graphite planes to diamond. Since the material is now definitely within the graphite-like region of the amorphous carbon phase diagram,[23] there is a large stress barrier to overcome to compress the layers together to form diamond. The stress level required is on the order of 80 GPa.[24] Note that to form ta-C from incident ions this barrier does not need to be overcome so that ta-C will form at a much lower value of stress than the barrier value.

A film corresponding to point B in Fig. 8 moves to a higher sp^3 fraction, contracting and reducing any strain energy present. The high density layers in the multilayer film as prepared lie close to point B and move as predicted to a slightly higher density. There have been several previous attempts to explain the stress relief in ta-C after annealing.[6–8] Our model explains in a simple way the driving force behind the stress release process and also explains the stress generation process in films of intermediate sp^3 fraction. The model also explains the stability of ta-C since there is a potential barrier between sp^3 and sp^2 rich phases.

In a multilayer structure of layers consisting of alternating layers indicated by points A and B (in Fig. 8), the annealing will introduce large changes in stress, with the low density layers developing stress and the high density layers relieving their stress. This leads to the large spatial variations in stress illustrated schematically in Fig. 6(d) which give rise to the observed preferred orientation effects.

IV. CONCLUSION

We have developed a model based on *ab initio* calculations which explains experimentally observed changes in stress and structure of amorphous carbon films following annealing in terms of minimization of free energy. The model predicts that ta-C films will reduce their stress and retain or even increase their level of sp^3 bonding. Films of intermediate sp^3 fraction are predicted to generate compressive stress and reduce their level of sp^3 bonding. The model also explains why the ta-C structure is stable following annealing. We have also observed the formation of preferred orientation

of graphitic planes as a response to stress in the absence of the dynamical phenomena that occur under ion bombardment. The preferred orientation in the vicinity of the interfaces in an annealed high sp^3/intermediate sp^3 multilayer film is explained as a consequence of the rapid spatial variations in stress near the interfaces.

ACKNOWLEDGMENTS

We would like to thank N. A. Marks (University of Sydney) for useful discussions and for performing the diamond calculation used in this work. We would also like to thank S. H. N. Lim (RMIT University).

[1] D. R. McKenzie, Rep. Prog. Phys. **59**, 1611 (1996).
[2] M. M. M. Bilek, D. R. McKenzie, R. N. Tarrant, S. H. M. Lim, and D. G. McCulloch, Surf. Coat. Technol. **156**, 136 (2002).
[3] B. K. Tay, D. Sheeja, and L. J. Yu, Diamond Relat. Mater. **12**, 185 (2003).
[4] D. Sheeja, B. K. Tay, L. J. Yu, and S. P. Lau, Surf. Coat. Technol. **154**, 289 (2002).
[5] J. P. Sullivan, T. A. Friedmann, and A. G. Baca, J. Electron. Mater. **26**, 1021 (1997).
[6] T. M. Alam, T. A. Friedmann, P. A. Schultz, and D. Sebastiani, Phys. Rev. B **67**, 245309 (2003).
[7] O. R. Monterio, J. W. Ager, D. H. Lee, K. C. Walter, and M. Nastasi, J. Appl. Phys. **88**, 2395 (2000).
[8] A. C. Ferrari, B. Kleinsorge, N. A. Morrison, A. Hart, V. Stolojan, and J. Robertson, J. Appl. Phys. **85**, 7191 (1999).
[9] D. G. McCulloch, D. R. McKenzie, and S. Prawer, Philos. Mag. A **72**, 1031 (1995).
[10] B. Rauschenbach and J. W. Gerlach, Cryst. Res. Technol. **35**, 675 (2000).
[11] D. R. McKenzie and M. M. M. Bilek, Thin Solid Films **382**, 280 (2001).
[12] L. Dong and D. J. Srolovitz, J. Appl. Phys. **84**, 5261 (1998).
[13] D. G. McCulloch, D. R. McKenzie, and C. M. Goringe, Phys. Rev. B **61**, 2349 (2000).
[14] X. Shi, Y. Q. Tu, H. S. Tan, B. K. Tay, and W. I. Milne, IEEE Trans. Plasma Sci. **24**, 1309 (1996).
[15] A. Anders, Surf. Coat. Technol. **93**, 158 (1997).
[16] G. G. Stoney, Proc. R. Soc. London, Ser. A **82**, 192 (1909).
[17] D. D. Berger, D. R. McKenzie, and P. J. Martin, Philos. Mag. Lett. **57**, 285 (1988).
[18] D. R. McKenzie and M. M. M. Bilek, J. Vac. Sci. Technol. A **16**, 2733 (1998).
[19] V. L. Solozhenko, I. A. Petrusha, O. Engler, and J. F. Bingert, J. Mater. Sci. **36**, 2659 (2001).
[20] K. F. McCarty, J. Vac. Sci. Technol. A **17**, 2749 (1999).
[21] R. F. Egerton, *Electron Energy-Loss Spectroscopy in the Electron Microscope*, 2nd ed. (Plenum, New York, 1996).
[22] J. L. Peng, X. D. Fan, and L. A. Bursill, Int. J. Mod. Phys. B **10**, 3875 (1996).
[23] D. G. McCulloch, D. R. McKenzie, and C. M. Goringe, J. Appl. Phys. **88**, 5028 (2000).
[24] S. Fahy, S. G. Louie, and M. L. Cohen, Phys. Rev. B **34**, 1191 (1986).